Stochastic variational approach to few-electron artificial atoms

K. Varga,[1,*] P. Navratil,[2,†] J. Usukura,[3] and Y. Suzuki[4]
[1]*Solid State Division, Oak Ridge National Laboratory, Oak Ridge, 37831 Tennessee and Institute for Nuclear Research of the Hungarian Academy of Sciences (ATOMKI), P. O. Box 51, 4000 Debrecen, Hungary*
[2]*Lawrence Livermore National Laboratory, P. O. Box 808, Livermore, California 94551*
[3]*Graduate School of Science and Technology, Niigata University, Niigata 950-2181, Japan*
[4]*Department of Physics, Niigata University, Niigata 950-2181, Japan*
(Received 17 October 2000; revised manuscript received 3 January 2001; published 23 April 2001)

The spectra of quantum dots of different geometries (quantum ring, quantum cylinder, spherical square well, and parabolic) are studied. The stochastic variational method on correlated Gaussian basis functions and a large scale shell-model approach have been used to investigate these ''artificial'' atoms and their properties in magnetic fields. Accurate numerical results are presented for $N=2-8$ electron systems.

DOI: 10.1103/PhysRevB.63.205308 PACS number(s): 73.61.−r, 85.35.Be

I. INTRODUCTION

Quantum dots[1–4] are solid state structures made of semiconductors or metals those confine a countable, small number of electrons into a small space. The observed properties of these confined electrons are similar to those of atoms. The possibility of fabrication of ''artificial atoms'' with ''tunable'' properties is a fascinating development in nanotechnology. These quantum dots not only offer the opportunity of various applications (laser and electronic devices, memories, quantum gates, etc.) but also are quite intriguing physical systems in their own right. Most theoretical model calculations use the effective-mass approximation to study the energy levels or other properties of the electrons confined in quantum dots. These calculations address the low-energy sector where the interband mixing is assumed to be negligible and the periodic crystal potential is taken into account through the effective mass and dielectric constant. In these models the electrons move in an external confining potential and interact via the Coulomb interaction.

Given the geometry of the quantum dot and the parameters of the heterostructure, the confining potential can be determined by a self-consistent calculation. This is not, however, a trivial task and most work on quantum dots uses simple model potentials. The confinement is generally very strong in the vertical z direction, creating quasi-two-dimensional (2D) systems. The confinement on the xy plane is most often assumed to be parabolic. A study of realistic confining potentials found that this approximation is fairly good in certain cases but generally the confining potential might significantly differ from a harmonic-oscillator one.[5] It is therefore important to investigate particular quantum dot geometries/structures as well.

The apparent similarity of ''natural'' atoms and quantum dots suggests the application of sophisticated theoretical methods used in atomic physics and quantum chemistry to calculate the properties of quantum dots. Parabolically confined 2D quantum dots have been studied by several different well-established methods: exact diagonalization techniques,[6–9] Hartree-Fock approximations,[10–12] and density functional approaches.[13,14] Quantum Monte Carlo (QMC) techniques have also been used for 2D,[15–17,19,20] as well as three-dimensional (3D) structures.[18] Few-electron artificial atoms of spherical[21,22] and cylindrical[23] symmetry in 3D have also been investigated in the variational and Hartree-Fock frameworks. The strongly correlated low-electronic-density regime got much attention due to the intriguing possibility of the formation of Wigner molecules.[12,24,25] Here we use a correlated basis function which gives very accurate results for different few-electron systems. The accuracy becomes important when one studies subtle properties such as level orders, weakly bound states, etc. We investigate different models of quantum dots suggested by various authors.

In this paper the stochastic variational method has been used to solve the few-electron Schrödinger equation. In this approach correlated Gaussians are adopted as basis functions. This basis is nonorthogonal and overcomplete. The trial function depends on the parameters of the Gaussians and one has to optimize the parameters to get the best energy. The most adequate basis functions are selected by the stochastic variational method (SVM).[26,27] The advantage of this basis lies in its flexibility. A relatively small number of basis functions give very accurate results provided that the parameters are carefully optimized.

To test the accuracy of the results we have expanded the wave function in terms of harmonic-oscillator Slater determinants as well. This basis forms a complete set and the energy is obtained by diagonalizing the corresponding eigenvalue problem. The only approximation is the truncation of the basis. The dimension of the harmonic-oscillator basis quickly increases with the number of single-particle states included and even the powerful Lanczos method becomes infeasible. The advantage of this approach is that it is simple. Once the matrix elements are calculated there is no need for optimization of the basis set. In addition, we may improve on this approach by utilizing the starting-energy-independent two-body effective interaction[28] that takes into account two-electron correlations from the excluded space. Again, no additional optimization is needed as the effective interaction does not depend on any extra parameter.

We have carefully compared the results obtained with these basis states to test the accuracy of the energies and other physical properties. These quantum mechanical systems provide us with very good tests of different approaches, and therefore we think that it is important and useful to tabulate the energy and other quantities of the quantum dots. This

may serve as a benchmark test to compare different methods.

An intriguing feature of these systems is that the strength (and shape) of the confining potential can be changed. Unlike in natural atoms the relative importance of the pairwise Coulomb interaction and the external potential can be tuned.

We have calculated the ground and the first few excited states. The ground and excited states are characterized by the total orbital angular momentum L and spin S. The order of the levels depends on the external (confining) potential. We have investigated how the level order changes as the parameter of the potential is varied.

The next section introduces the basics of our formalism. The results of the calculation for different systems are presented in Sec. III. The last section is devoted to discussion and summary.

II. THE FORMALISM

We investigate a system of N_e electrons confined by the potential $V_{\rm con}(\mathbf{r})$. The Hamiltonian is

$$H=\sum_{i=1}^{N_e}\left(-\frac{\hbar^2}{2m^*}\nabla_i^2+V_{\rm con}(\mathbf{r}_i)\right)+\frac{e^2}{\epsilon}\sum_{i<j}^{N_e}\frac{1}{|\mathbf{r}_i-\mathbf{r}_j|}. \quad (1)$$

In Eq. (1), m^* is the effective mass of the electron and ϵ is the dielectric constant of the semiconductor. In the following (if not explicitly specified otherwise) we will use effective atomic units, defined by $\hbar=e^2/\epsilon=m^*=1$. In this system of units, the length unit is the Bohr radius ($a=\hbar^2/m_e e^2$) times $\epsilon/(m^*/m_e)$, and the energy unit is the Hartree ($H=m_e e^4/\hbar^2$) times $(m^*/m_e)/\epsilon^2$ where m_e is the mass of the electron. For the GaAs dots we consider here, $\epsilon=12.4$ and $m^*=0.067m_e$, and the effective Bohr radius a_0^* and the effective Hartree H^* are $\simeq 97.94$ Å and $\simeq 11.86$ meV, respectively. These effective length and energy units are called atomic units (a.u.) in what follows.

In the variational method the trial wave function is expanded in terms of basis functions:

$$\Psi=\sum_i c_i\Phi_i, \quad (2)$$

and the variational energies are obtained by solving the generalized eigenvalue problem

$$\sum_j (H_{ij}-EO_{ij})c_j=0, \quad H_{ij}=\langle\Phi_i|H|\Phi_j\rangle$$

and

$$O_{ij}=\langle\Phi_i|\Phi_j\rangle. \quad (3)$$

The energy eigenvalues $E_1, E_2, \ldots$ are variational upper bounds of the energies of the ground and first, second, ... excited states.

A. Correlated Gaussian basis functions

The correlated Gaussian basis is defined in the following way:

$$\Phi_i(\mathbf{r})=\mathcal{A}\left\{\exp\left(-\frac{1}{2}\mathbf{r}A_i\mathbf{r}\right)\theta_{LM_L}(\mathbf{r})\chi_{SM_S}\right\}, \quad (4)$$

where $\mathcal{A}$ is the antisymmetrizing operator for the electrons and $\mathbf{r}=(\mathbf{r}_1,\ldots,\mathbf{r}_{N_e})$ stands for a set of spatial coordinates of the electrons. $\mathbf{r}A_i\mathbf{r}$ is a short hand notation of the quadratic form $\Sigma_{j,k=1}^{N_e}(A_i)_{jk}\mathbf{r}_j\cdot\mathbf{r}_k$, where A_i is an $N_e\times N_e$ symmetric positive-definite matrix whose elements are variational parameters. Both the spin function χ_{SM_S} and the angular function $\theta_{LM_L}(\mathbf{r})$ are constructed by successively coupling the corresponding single-particle functions:

$$\chi_{SM_S}=[[[\xi_{1/2}(1)\xi_{1/2}(2)]_{s_{12}}\xi_{1/2}(3)]_{s_{123}}\ldots]_{SM_S} \quad (5)$$

and

$$\theta_{LM_L}(\mathbf{r})=[[[\mathcal{Y}_{l_1}(\mathbf{r}_1)\mathcal{Y}_{l_2}(\mathbf{r}_2)]_{l_{12}}\mathcal{Y}_{l_3}(\mathbf{r}_3)]_{l_{123}}\ldots]_{LM_L}, \quad (6)$$

where $\xi_{m/2}$ and $\mathcal{Y}_{lm}(\mathbf{r})=r^l Y_{lm}(\hat{\mathbf{r}})$ are the spin and angular functions of the electron.

The Hamiltonian we consider in this paper contains no term that couples the spin and orbital angular momenta, and commutes with the total spin and total orbital angular momenta or their z components when the uniform magnetic field is applied in the z direction. There is no coupling between the spin and the orbital part in the basis function of Eq. (4).

The correlated Gaussian function can be rewritten in a more intuitive form:

$$\exp\left(-\frac{1}{2}\mathbf{r}A\mathbf{r}\right)=\exp\left(-\frac{1}{2}\sum_{k<l}^{N_e}\alpha_{kl}(\mathbf{r}_k-\mathbf{r}_l)^2-\frac{1}{2}\sum_{k=1}^{N_e}\beta_k\mathbf{r}_k^2\right). \quad (7)$$

α_{kl} and β_k can be expressed by the elements of A and vice versa. The advantage of this notation is that it explicitly connects the nonlinear parameters α_{ij} to the pair correlation between the particles i and j and thus explains the name ''correlated Gaussians.'' The second part, $\exp(-\frac{1}{2}\Sigma_{k=1}^{N_e}\beta_k\mathbf{r}_k^2)$, is a product of independent single-particle Gaussians.

B. Stochastic variational method

The energy crucially depends on the variational parameters. The optimal nonlinear parameters are selected by the stochastic variational method.[26,27] In each step of this procedure, $\mathcal{K}$ different A_i are generated by randomly choosing the values of α_{kl} and β_k from the $[0,\beta]$ interval. The parameter set that gives the best variational energy is selected and the function corresponding to that parameter set is added to the set of basis functions. The trial function also depends on the intermediate coupling quantum numbers $(s_{12},s_{123},\ldots)$ and $(l_1,l_2,l_{12},l_3,\ldots)$. These possibilities are also randomly tested during the optimization of the basis.

Our stochastic selection procedure uses the following steps.

(1) Setting up a new basis or enlarging an existing one. Let us assume that the basis set has $\mathcal{N}-1$ elements. One generates $\mathcal{K}$ random basis states and calculates the energies

$E_{\mathcal{N}i}$ $(i=1,\ldots,\mathcal{K})$ with the new $\mathcal{N}$-dimensional bases that contain the ith random element and the preselected $\mathcal{N}-1$ basis elements. The random state that gives the lowest energy is selected as a new basis state and added to the basis. The variational principle ensures that the energy of the $\mathcal{N}$-dimensional basis is always lower than that of the $(\mathcal{N}-1)$-dimensional one. This procedure is therefore guaranteed to lead to a better and better upper bound of the ground state energy. Notice that as the $(\mathcal{N}-1)$-dimensional basis is orthogonalized this method does not require the diagonalization of $\mathcal{N}$-dimensional matrices.[26,27] The energy gain $\epsilon_{\mathcal{N}}=E_{\mathcal{N}}-E_{\mathcal{N}-1}$ shows the rate of convergence. A calculation of good convergence gives $\epsilon_{\mathcal{N}}\approx 0$.

(2) Refinement: Improving the energy of a basis. In the previous step only the newly added element is optimized, but the rest of the basis is kept fixed. In the refinement we keep the dimension of the basis fixed and try to replace the kth basis element with $\mathcal{K}$ randomly generated elements. If the best energy obtained by substituting the kth basis state with the random candidate is lower than that of the original basis, then the kth basis state is discarded and the new random state is included in the basis. This procedure is cyclically repeated for $k=1,\ldots,\mathcal{N}$. As the dimension of the model space is fixed, this step does not necessarily give lower energy, but in practice in most cases it does. Actually, if one cannot find better basis elements, that is an indication of a well-converged energy/basis. Again no diagonalization is needed in this step when starting from an orthogonalized basis.

(3) Optimization by ''fine tuning'' of the parameters. In step 2 the parameters are randomly selected irrespective of their previous values. This certainly helps to avoid the traps of local minima, but if one is already (presumably) close to the ''global'' minimum then the chance to move closer to it is small. If the basis parameters are ''reasonably'' optimized or further repetition of step 1 or 2 does not lead to appreciable changes, one may try to change the basis parameters by selecting new parameters in the vicinity of the existing ones. That increases the probability of finding the nearby minimum. In practical calculations this step was implemented by requiring the new random parameters to be in the $[0.8\alpha,1.2\alpha]$ interval (α is the previously chosen parameter). In this case the basis optimization is done in exactly the same way as in step 2. The only difference is that the search interval is limited and defined by the previous parameters.

A combination of steps 1, 2, and 3 is repeated until the required accuracy is reached. A practical and economical way to set up a basis is to generate $\mathcal{N}$ elements ($\mathcal{N}=20$ or 40 is a reasonable choice) by using step 1. Then repeat step 2 for each basis state several (say 3–5) times. Use step 1 once more to enlarge the basis by adding $\mathcal{N}$ elements to it and repeat step 2 as described before. After reaching a certain basis size where further repetition of steps 1 and 2 does not yield considerable improvement, then try step 3.

This basis selection procedure proved to be quite reliable and provides a very accurate solution. More details can be found in Ref. 26.

C. Harmonic-oscillator basis

Alternatively, we also set up a harmonic-oscillator basis.[29] In this case the basis functions are

$$\Phi_i(\mathbf{r})=\det\{[\varphi_{n_j l_j m_j}(\mathbf{r}_j)\xi^1_{\frac{1}{2}\mu_j}(j)]\}, \tag{8}$$

where the single-particle function $\varphi_{n_j l_j m_j}$ is a harmonic-oscillator function. This basis depends on only one parameter, the harmonic-oscillator width. For harmonic-oscillator confinement this is chosen to be equal to the oscillator frequency of the potential. In this way the harmonic-oscillator basis functions are eigenfunctions for a noninteracting system.

This is an orthogonal basis and the Hamiltonian matrix is sparse. The Lanczos method, in particular the many-fermion dynamics shell-model code,[30] is used to find the lowest eigenvalues. In the diagonalization we used all states up to $\Sigma_{i=1}^{N_e}(2n_i+l_i)\leqslant N_{\max}$.

The basic difference between the two bases is that the Gaussian basis is *explicitly* correlated. It explicitly depends on the $|\mathbf{r}_i-\mathbf{r}_j|$ distances, so it is better suited to describe the electron-electron correlations. At the same time the harmonic-oscillator basis is simpler because no optimization is needed.

An advantage of the harmonic-oscillator basis is the fact that we may alternatively perform the calculations in the Jacobi coordinates with the center-of-mass degrees of freedom removed. It is straightforward, although numerically intensive, to construct an antisymmetrized harmonic-oscillator basis depending on the Jacobi coordinates.[28] Depending on the problem, we may choose the more efficient basis. For $N_e=3,4,5$ electron systems it turns out that the use of Jacobi coordinates is more profitable. For larger numbers of electrons, it is more efficient to use the single-particle coordinates and the Slater determinant basis (8).

As the harmonic-oscillator frequency is fixed as described above, the only parameter of the calculation is the model space size characterized by $N_{\max}$. In the present calculations we use as large $N_{\max}$ as possible, typically $N_{\max}=15$–33 for $N_e<5$ and $N_{\max}=8$–12 for larger systems.

A speed-up of convergence can be achieved by utilizing the effective-interaction approach that was successfully applied in *ab initio* shell-model calculations for few-nucleon systems and light nuclei.[28,29] While it is crucial in the nuclear physics application to use the effective interactions, in the present electron systems the effective interaction provides only minor improvement. In some cases, however, it brings the SVM and SM results to much closer agreement. The details of how the effective interaction is computed from the bare Hamiltonian, here the harmonic-oscillator and Coulomb interaction, is given, e.g., in Refs. 28 and 29. The basic goal of the effective interaction is to take into account, in this case two-electron, correlations from the excluded space, i.e., from the space containing excitations above $N_{\max}$. A formal difference from the nuclear case is that here the harmonic-oscillator potential is a real binding potential, while in the nuclear application it is a model potential representing the mean field formed by all nucleons, which is added/subtracted to the real nucleon-nucleon interaction in order to facilitate the effective interaction calculation.

We note that when the basis (8) is used the good quantum numbers are checked by evaluating the mean values of relevant operators, e.g., J^2, **L**, and **S**, for each eigenstate.

D. Magnetic field

In external magnetic field the kinetic energy operator is replaced by

$$\frac{1}{2m^*}\mathbf{p}_i^2 \rightarrow \frac{1}{2m^*}\left(\mathbf{p}_i+\frac{e}{c}\mathbf{A}_i\right)^2. \tag{9}$$

We consider a uniform magnetic field $\mathbf{B}=(0,0,-B)$. By taking $\mathbf{A}_i=-\frac{1}{2}\mathbf{r}_i\times\mathbf{B}$ the above expression can be rewritten in a more detailed form:

$$\frac{1}{2m^*}\left(\mathbf{p}_i+\frac{e}{c}\mathbf{A}_i\right)^2 = -\frac{1}{2m^*}\hbar^2\Delta_i+\frac{1}{2}m^*(\omega_c/2)^2(x_i^2+y_i^2) - \frac{1}{2}\omega_c l_{zi}, \tag{10}$$

where l_{zi} is the z component of the orbital angular momentum of the ith electron. The cyclotron frequency for the parameters we use in this paper reads as

$$\hbar\omega_c=\frac{e\hbar B}{m^*c}=\frac{2m_e}{m^*}\mu_B B=0.145\,72B(H^*), \tag{11}$$

where the Bohr magneton is $\mu_B=e\hbar/(2m_e c)=0.057\,88$ meV/T. The interaction of the magnetic field with the spins leads to the Zeeman term $-g^*\mu_B B s_{zi}$, where s_{zi} is the z component of the spin of the ith electron and g^* is the effective g factor of the electron. The Zeeman term leads to the splitting of the energies for different spin orientations. As the Hamiltonian with this term still commutes with the z component of the total spin, $S_z=\Sigma_{i=1}^{N_e}s_{zi}$, the energy shift is simply given by $-g^*\mu_B B S_z$ and one can easily add this to the energies presented in the following. This energy is not included in what follows.

The correlated Gaussians defined above are not ideally suited for systems in magnetic field, because the basis functions belonging to different orbital angular momenta would be coupled by the Hamiltonian. This coupling would require an infinite series of orbital angular momentum states, which is obviously out of the question. To avoid this, we choose a deformed form of the correlated Gaussian (DCG):[31]

$$\exp\left\{-\frac{1}{2}\sum_{i,j=1}^{N_e}A_{ij}\rho_i\cdot\rho_j-\frac{1}{2}\sum_{i,j=1}^{N_e}B_{ij}z_i z_j\right\}, \tag{12}$$

where the nonlinear parameters are different (and independent) in the xy and z directions $[\rho_i=(x_i,y_i)]$. This extension brings a great deal of flexibility by allowing a separate description on the xy plane and along the z axis. The Hamiltonian does not commute with L^2 but it does with L_z. The eigenfunctions have good quantum number M of L_z. Note that we will use M for the orbital angular momentum quantum number in 2D and L for the one in 3D. The above form of the DCG belongs to $M=0$. To allow for $M\neq 0$ states we multiply the basis by[26]

$$\prod_{i=1}^{N_e}\xi_{m_i}(\rho_i), \tag{13}$$

where

$$\xi_m(\rho)=\begin{cases}(x+iy)^m & \text{for non-negative integer } m\\ (x-iy)^{-m} & \text{for negative integer } m.\end{cases} \tag{14}$$

Thus our variational basis function reads as

$$\Phi_M(\mathbf{r})=\mathcal{A}\left\{\left(\prod_{i=1}^{N_e}\xi_{m_i}(\rho_i)\right)\times\exp\left(-\frac{1}{2}\sum_{i,j=1}^{N_e}A_{ij}\rho_i\cdot\rho_j-\frac{1}{2}\sum_{i,j=1}^{N_e}B_{ij}z_i z_j\right)\right\}, \tag{15}$$

where $M=m_1+m_2+\cdots+m_{N_e}$.

The above basis is defined for 3D cases. It is used not only for solutions in the presence of magnetic field but also for external potentials with cylindrical symmetry. For 2D calculations the same form is used except that the third component of the vectors is dropped (or equivalently $B_{ij}=0$ is assumed).

III. CALCULATION

A. Harmonic-oscillator confinement in 2D

Harmonically confined 2D systems have received much theoretical attention and this is a very good test case to gauge the accuracy of different approaches. In this case the confining interaction takes the simple $V_{\rm con}(r)=\frac{1}{2}m^*\omega^2 r^2$ form.

TABLE I. Comparison of the energies of harmonically confined 2D three-electron system ($\omega=0.2841$, $\hbar\omega=3.37$ meV) by different methods. The energies are given in meV. Values in parentheses are given in atomic units.

		QMC			
(M,S)	SVM	Diag. Ref. 6	Ref. 15	Ref. 17	Ref. 16
(1,1/2)	26.7827 (2.2582)	26.82	26.77	26.8214±0.0036	26.88
(2,1/2)	28.2443 (2.3814)	28.27	28.30		28.35
(3,3/2)	30.0101 (2.5304)	30.02	30.04		30.03

TABLE II. Comparison of the energies of harmonically confined 2D electron systems ($\omega=0.28, \hbar\omega=3.32$ meV) by different methods. η is the virial factor.

N_e	(M,S)	QMC (Ref. 17)	SVM	η
2	(0,0)	1.02162(7)	1.02164	0.999995
3	(1,1/2)	2.2339(3)	2.2320	0.999988
4	(0,1)	3.7157(4)	3.7130	0.999971
4	(2,0)	3.7545(1)	3.7525	0.999982
4	(0,0)	3.7135(6)	3.7783	0.999992
5	(1,1/2)	5.5336(3)	5.5310	0.999481
6	(0,0)	7.5996(8)	7.6020	0.998912

The single-particle energy of the harmonic-oscillator potential is given by $(2n+|m|+1)\hbar\omega$, where $n=0,1,2,\ldots$, and $m=0,\pm1,\pm2,\ldots$. In Table I we compare our results to the ''exact diagonalization''[6–8] and QMC methods[15–17] for the $N_e=3$ electron system. We have carefully optimized the parameters and repeated the calculation several times to check the convergence. Our result is expected to be accurate up to the digits shown in Table I. In principle the QMC calculations, except for the statistical error, give the exact energy of the system. In practical cases the famous ''minus-sign problem'' forces the QMC approaches to use certain approximations (in Refs. 16 and 17 the ''fixed-node'' method has been used). The slight difference between our results and the QMC values is probably due to this fact. The energies for both the ground and excited states are in good agreement. Our results are slightly better than the other calculations in each case.

In Table II a similar comparison is presented for $N_e=2$–6 electron systems. The QMC results[17] quoted in Table II are obtained by very careful calculations and their statistical error is very small. Note that the confining strength is slightly different in the calculations presented in Tables I and II. This table also includes the virial factor

$$\eta=2\langle T\rangle/\langle W\rangle, \quad \langle W\rangle=\left\langle \sum_{i=1}^{N_e} \mathbf{r}_i\cdot\boldsymbol{\nabla}_i V_{\rm int}\right\rangle, \tag{16}$$

where $V_{\rm int}$ is the ''interaction part'' of the Hamiltonian, including the confining and the electron-electron interactions. The virial factor is unity for the exact wave function.

Our result is in excellent agreement with the QMC predictions[17] in all but one case ($N_e=4$). The QMC method renders the $(M,S)=(0,0)$ state as the ground state and the $(M,S)=(0,1)$ state as the first excited state, which is a violation of Hund's rule. The shell filling and Hund's rule have been experimentally investigated in Ref. 2 and it is found that a circular dot obeys Hund's rule. According to Hund's rule the ground state of a system with a well-developed shell structure is in the maximum spin state allowed by the Pauli principle. The violation of Hund's rule in this system was also observed in another QMC calculation.[15] This latter calculation predicts a relatively large energy difference between the (0,0) and (0,1) levels, but it is somewhat less accurate for $N_e=4$, using only the lowest Landau levels.

Our calculations, in agreement with Hund's rule, predict the $(M,S)=(0,1)$ state to be the ground state and the (2,0) and (0,0) states to be the lower excited states. This contradicts the results of Refs. 15 and 17 but is in agreement with the other QMC calculation.[16] The violation of Hund's rule for $N_e=4$ is also found in unrestricted Hartree-Fock calculations,[12] while exact diagonalization calculations[8] show that the shell filling obeys Hund's rule.

Our other energies are very close to the QMC results: The agreements for $N_e=5$ and $N_e=6$ electron systems are very impressive.

We define the pair correlation function

$$P(\mathbf{r},\mathbf{r}_0)=\frac{2}{N_e(N_e-1)} \times\langle\Psi|\sum_{i<j}\delta(\mathbf{r}_i-\mathbf{R}-\mathbf{r})\,\delta(\mathbf{r}_j-\mathbf{R}-\mathbf{r}_0)|\Psi\rangle. \tag{17}$$

Here $\mathbf{r}_0$ is a fixed vector and its magnitude is chosen to be equal to $\langle\Psi|\Sigma_i|\mathbf{r}_i-\mathbf{R}||\Psi\rangle/N_e$. The function $P(\mathbf{r},\mathbf{r}_0)$ gives us information on where one electron located at $\mathbf{r}_0$ experiences other electrons. Figures 1 and 2 display the pair correlation functions for the ground state $(M,S)=(1,1/2)$ and the first excited state $(M,S)=(2,3/2)$ of the $N_e=5$ electron system. Both figures show qualitatively similar features. For $\omega=1$, the confinement potential is strong and the contribution of the single-particle energies to the total energy is larger than that of the Coulomb potential. The electrons are confined in a rather compact region so that the contour map does not show four clear peaks. On the contrary, for $\omega=0.1$ the effect of the confinement becomes weak and the contribution of the Coulomb potential is larger than that of the harmonic-oscillator part. The size of the system grows and we see clearly a well-separated pentagonlike structure. The Wigner-molecule-like structures formed in this case are in very good qualitative agreement with the results of Ref. 12.

Next we present in Table III an example where the magnetic field is nonzero. Again, the energies are in good agreement with those from the QMC (Ref. 15) and diagonalization[6] methods. In 2D the inclusion of the magnetic field leads to a change of the harmonic-oscillator frequency

$$\omega\rightarrow\sqrt{\omega^2+(\omega_c/2)^2} \tag{18}$$

and an energy shift by $-\frac{1}{2}M\hbar\omega_c$, so we expect that our results are as accurate as those for the zero field case. The accuracy is also indicated by the virial factor included in Table III.

We have improved the prediction of the diagonalization method.[6] The diagonalization method would give the ''exact'' solution in infinite model space. In practice the diagonalization is always limited to finite dimensions. The slight disagreement between our and the QMC results might be due to the statistical (and/or fixed-node) error of the QMC calculation.

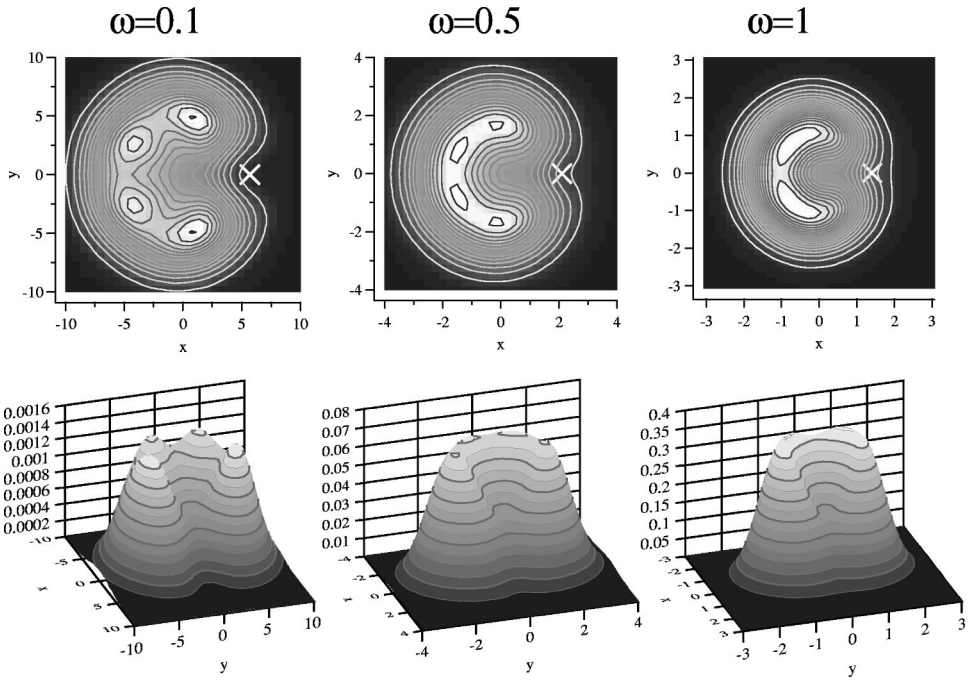

FIG. 1. Pair correlation function of the ground state $(M,S)=(1,1/2)$ of 2D five-electron system as a function of the frequency ω of the harmonically confining potential. The white cross denotes $\mathbf{r}_0$. Atomic units are used.

The energy levels of the first three spin-polarized and spin-unpolarized three-electron states in a magnetic field are shown in Fig. 3. The spin-unpolarized $(1,1/2)$ state is the ground state in the weak magnetic field limit. The level order at $B=0$ is $(1,1/2),(0,3/2),(2,1/2),(0,1/2),(3,3/2)$. The $M=0$ states are formed by placing one electron in each of the $m=0,1,-1$ single-particle orbits. The $(2,1/2)$ unpolarized state becomes the ground state in a very small interval of the magnetic field strength. The sequence of ground states on increasing the magnetic field is $(1,1/2),(2,1/2),(3,3/2),(4,1/2),(6,3/2)$ in agreement with Ref. 7 [the $(4,1/2)$ state is not included in Fig. 3]. The lowest spin-polarized state is the $(0,3/2)$ state for weak field. For stronger field the $(3,3/2)$ and then the $(6,3/2)$ states become the lowest spin-polarized (and ground) state, following the $(3,6,\ldots,3n)$ ''magic'' sequence. Other spin-polarized states [e.g., $(1,3/2)$, etc.] never become the lowest state. The explanation of the magic sequence is very simple. In the spin-polarized case all electrons have to occupy different orbits. As the magnetic field gets stronger, the single-particle states belonging to positive orbital angular momentum quantum numbers $(m_i=0,1,2,3,\ldots)$ are energetically more favorable than those with negative ones. The $M=3$ state $[(m_1,m_2,m_3)=(0,1,2)]$ is therefore lower than the $M=2$ state [which

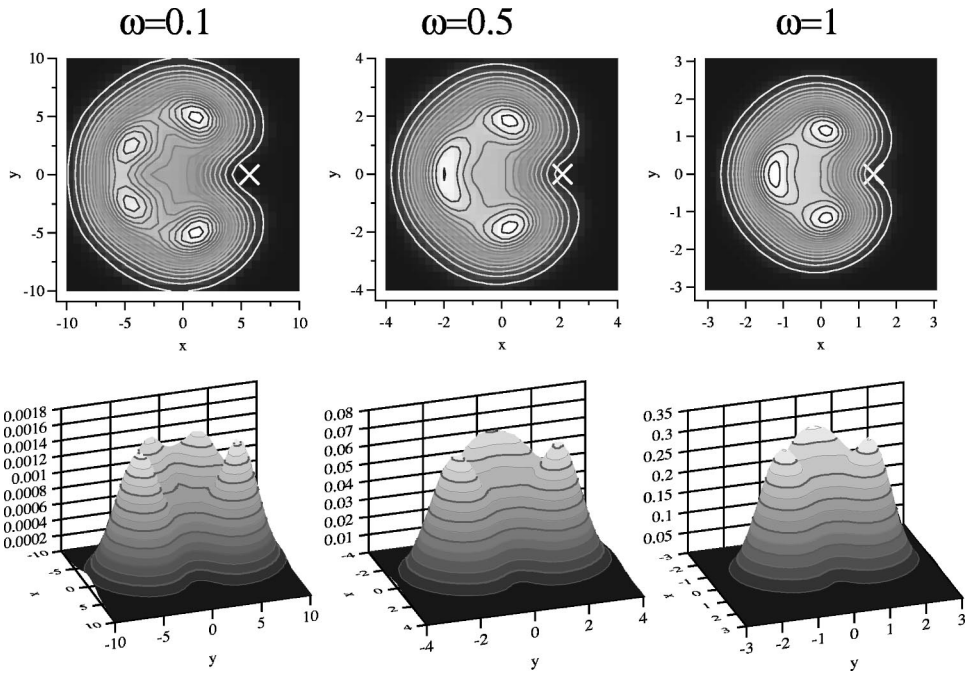

FIG. 2. Pair correlation function of the excited state $(M,S)=(2,3/2)$ of 2D five-electron system as a function of the frequency ω of the harmonically confining potential. The white cross denotes $\mathbf{r}_0$. Atomic units are used.

TABLE III. Comparison of the energies of harmonically confined 2D three-electron systems in magnetic field ($\omega=0.2841$) by different methods. The energies are in meV except for the values in parentheses which are in atomic units. η is the virial factor.

(M,S)	B (T)	SVM	η	QMC (Ref. 15	Diag. (Ref. 6)
(1,1/2)	0.0	26.78 (2.2582)	0.999991	26.77	26.82
(1,1/2)	1.0	26.61 (2.2442)	0.999989	26.60	26.65
(1,1/2)	2.0	27.69 (2.3353)	1.000034	27.68	27.74
(1,1/2)	3.0	29.71 (2.5055)	0.999987	29.69	29.77
(1,1/2)	4.0	32.36 (2.7283)	1.000026	32.32	32.43
(1,1/2)	5.0	35.39 (2.9842)	0.999985	35.33	35.48
(2,1/2)	0.0	28.24 (2.3814)	0.999992	28.30	28.27
(2,1/2)	1.0	27.28 (2.2998)	0.999925	27.33	27.29
(2,1/2)	2.0	27.67 (2.3338)	0.999905	27.72	27.69
(2,1/2)	3.0	29.09 (2.4531)	0.999954	29.14	29.13
(2,1/2)	4.0	31.22 (2.6324)	0.999976	31.26	31.26
(2,1/2)	5.0	33.79 (2.8495)	0.999963	33.82	33.85
(3,3/2)	0.0	30.01 (2.5304)	0.999999	30.04	30.02
(3,3/2)	1.0	28.24 (2.3817)	1.000006	28.27	28.25
(3,3/2)	2.0	27.97 (2.3585)	0.999997	28.00	27.98
(3,3/2)	3.0	28.83 (2.4315)	0.999999	28.86	28.85
(3,3/2)	4.0	30.48 (2.5703)	0.999997	30.51	30.50
(3,3/2)	5.0	32.63 (2.7519)	0.999998	32.67	32.66

requires $(0,-1,3)$ or $(1,2,-1)$, etc.]. For a weak magnetic field the above argument does not hold in general and the lowest polarized state is $M=0$ with the $(0,1,-1)$ orbits.

A similar picture is valid for $N_e=4$ (see Fig. 4). In the very weak field regime the unpolarized $(M,S)=(0,1)$ state is the ground state. On increasing the magnetic field, the spin-polarized $M=2$ state $[(m_1,m_2,m_3,m_4)=(0,1,-1,2)]$ becomes the ground state before the ''magic'' $M=6(0,1,2,3)$ state takes over.

Figure 4 reassures us that the $(M,S)=(0,1)$ state is the ground state and the $(M,S)=(0,0)$ is an excited state for zero magnetic field: Both states belong to $M=0$, and therefore the change of the magnetic field simply changes the harmonic-oscillator frequency [see Eq. (18)]. The figure thus

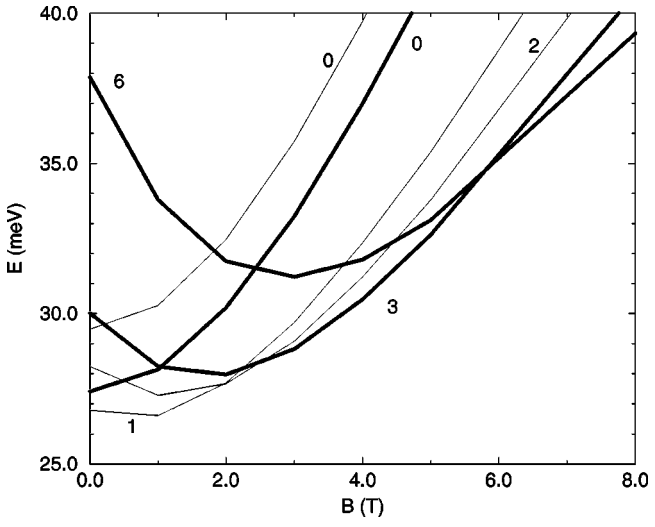

FIG. 3. Energies of the harmonically confined ($\hbar\omega=3.37$ meV) lowest spin-unpolarized ($S=1/2$, thin solid line) and spin-polarized ($S=3/2$, thick solid line) three-electron states in a magnetic field. The orbital angular momentum M of the state is indicated by the number next to the curve. The Zeeman energy is not included.

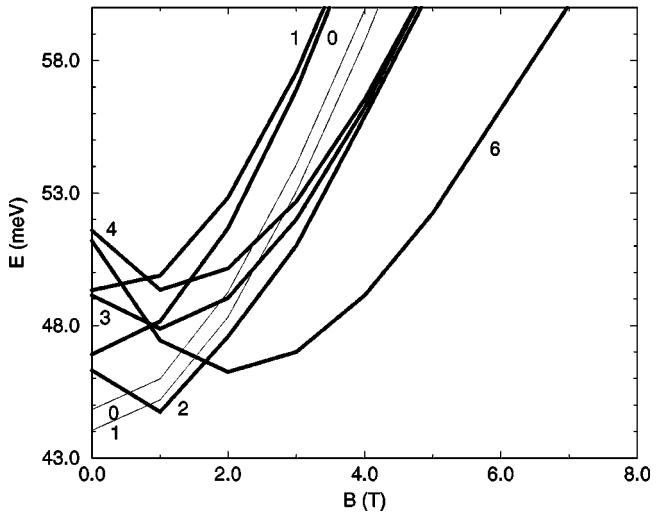

FIG. 4. Energies of the harmonically confined ($\hbar\omega=3.37$ meV) lowest spin-polarized ($S=2$, thick solid line) four-electron states in a magnetic field. The orbital angular momentum M of the state is indicated by the number next to the curve. The two thin solid curves are the $S=0$ and $S=1$ states belonging to $M=0$ (these S values are indicated next to the thin curves). The Zeeman energy is not included.

TABLE IV. Energies of harmonically confined two-electron system in 3D.

	ω		
(L,S,π)	0.01	0.5	10
$(0,0,+)$	0.07921	2.0000	32.449
$(1,1,-)$	0.08198	2.3597	41.665
$(2,0,+)$	0.08681	2.7936	51.338
$(0,0,+)$	0.09696	2.9401	52.072
$(3,1,-)$	0.09302	3.2538	61.149
$(1,1,-)$	0.10005	3.3286	61.504

shows that the order of these two states remains the same for different harmonic-oscillator frequencies.

B. Harmonic-oscillator confinement in 3D

We have calculated the energies of the ground and first few excited states of 3D few-electron systems confined by a harmonic-oscillator potential $[V_{\rm con}(r)=\frac{1}{2}m^*\omega^2r^2]$. The results for different values of the oscillator frequency are compared in Tables IV–X. All intermediate spin coupling possibilities $(s_{12},s_{123},\ldots)$ are included in the trial function. The partial wave components $(l_1,l_2,\ldots)$ are included up to $\Sigma_{i=1}^{N_e-1}l_i\leqslant 6$. The quantum numbers necessary to specify the states are the total orbital momentum L, the total spin S, and the parity π.

The two-electron case is relatively simple and it is analytically solvable for certain frequencies.[32] For $\omega=0.5$, for example, the exact energy is 2 a.u.,[32] and we can easily reproduce this value up to several digits as shown in Table IV, where the energies of other low-lying states are also listed. Three very different oscillator frequencies are used to test the accuracy of the method under different circumstances. In the case of $\omega=0.01$ the confinement is extremely weak and the Coulomb interaction governs the dynamics. In the other limiting case the confinement is very strong ($\omega=10$). Another reason for choosing these values is that we want to study the ordering of the energy levels as a function of the strength of the confining interaction. In the two-electron case, for example, there is a level crossing between the state $(L,S,\pi)=(3,1,-)$ and the first excited state of $(0,0,+)$. The order of the other levels listed in Table IV does not change.

The energies of the ground and excited states calculated by the correlated Gaussian and the harmonic-oscillator shell-model bases are compared for $N_e=3$–6 electron systems in Tables V–VIII. Both methods give very similar results. The agreement is especially good for the ground and first excited states. For higher excited states the Gaussian basis gives slightly less accurate energies because it is significantly more difficult to optimize the basis for excited states. In addition to the present results we note that the harmonic-oscillator calculation dependence on the model space size for $N_e=3,4$ and $\omega=0.5$ was discussed and tabulated in Ref. 33.

The agreement is especially striking for $N_e=3$. Almost all digits are equal for most of the calculated cases. It is interesting to compare the order of the states in 2D and 3D. In the 2D case for $N_e=3$ the energy levels of the first few states follow the order of $(M,S)=(1,1/2),(0,3/2),(2,1/2),(0,1/2)$, while in 3D the levels are ordered as $(L,S,\pi)=(1,1/2,-),(1,3/2,+),(2,1/2,+),(0,1/2,+)$. This shows that the lowest levels are built up from the same single-particle states. In the 3D ground state two electrons are in the $l=0$ orbital and one is in the $l=1$ orbital. The first excited state has two electrons in the $l=1$ orbital, which are coupled to $L=1$ because their spin must be parallel to build up $S=3/2$ with the third. In the 2D case they are in the $m=1$ and $m=-1$ orbitals and their total orbital angular momentum is $M=0$. The higher excited states have similar correspondence. The same similarity occurs for $N_e=4$ $[(M,S)=(0,1),(2,0),(0,0)$ in 2D and $(L,S,\pi)=(1,1,+),(2,0,+),(0,0,+)$ in 3D]. For example, the 3D ground state has two electrons in the $l=0$ and two electrons (with parallel spin) in the $l=1$ orbital and the two electrons in the $l=1$ orbital are again coupled to $L=1$. In the 2D ground state the two electrons are in the $m=1$ and $m=-1$ orbitals and the orbital angular momentum is $M=0$. With respect to the single-particle state occupations there is of course a big difference between the 2D and 3D cases. In 2D the shell fillings occur at $N_e=2,6,12,20,\ldots$, etc., while in 3D the shells are filled at $N_e=2,8,20,40,\ldots$. For $N_e>6$ particle systems the single-particle components of the wave functions in 2D and 3D might be quite different.

TABLE V. Energies of harmonically confined three-electron system in 3D. The SVM is the stochastic variational calculation, SM is the shell model, and SM-eff is the shell model with effective-interaction approach (see Sec. II D). Atomic units are used.

	SVM	SM-eff	SM	SVM	SM-eff	SM	SVM	SM-eff	SM
(L,S,π)		$\omega=0.01$			$\omega=0.5$			$\omega=10$	
$(1,1/2,-)$	0.181936	0.181936	0.181936	4.013240	4.013224	4.013511	61.138525	61.138549	61.139485
$(1,3/2,+)$	0.182973	0.182973	0.182973	4.310690	4.310690	4.310712	69.972571	69.972571	69.972624
$(2,1/2,+)$	0.184585	0.184584	0.184584	4.366473	4.366385	4.366537	70.315335	70.315387	70.315871
$(0,1/2,+)$	0.191567	0.191568	0.191568	4.467439	4.467459	4.467878	70.853077	70.853154	70.854399
$(2,1/2,-)$	0.198201	0.187935	0.187935	4.717817	4.717817	4.717828	79.490651	79.490655	79.490680
$(1,3/2,-)$	0.193764	0.193764	0.193764	4.794580	4.794582	4.794614	79.860576	79.860582	79.860650
$(1,1/2,-)$	0.193351	0.193325	0.193325	4.805341	4.797973	4.798186	79.890842	79.890818	79.891346
$(1,1/2,-)$	0.199667	0.199656	0.199656	4.960409	4.957257	4.957683	80.793524	80.793567	80.794750

TABLE VI. Energies of harmonically confined four-electron system in 3D. See the caption of Table V.

(L,S,π)	SVM	SM-eff $\omega=0.01$	SM	SVM	SM-eff $\omega=0.5$	SM	SVM	SM-eff $\omega=10$	SM
(1,1,+)	0.3159	0.3141	0.3141	6.3492	6.3490	6.3502	91.4466	91.4459	91.4496
(2,0,+)	0.3177	0.3188	0.3189	6.3865	6.3865	6.3896	91.6750	91.6758	91.6847
(0,0,+)	0.3210	0.3185	0.3185	6.4462	6.4456	6.4474	92.0260	92.0239	92.0297
(0,2,−)	0.3138	0.3151	0.3151	6.5875	6.5875	6.5879	99.9068	99.9041	99.9053
(2,0,−)	0.3198	0.3181	0.3181	6.7002	6.6961	6.6980	100.5877	100.5875	100.5930
(1,1,−)	0.3240	0.3195	0.3195	6.7196	6.7093	6.7105	100.6478	100.6199	100.6235
(1,0,−)	0.3278	0.3251	0.3251	6.7961	6.7935	6.7963	101.0946	101.0740	101.0813
(1,1,−)	0.3408	0.3232	0.3232	6.8448	6.8153	6.8169	101.3253	101.2220	101.2270
(2,2,+)	0.3223	0.3212	0.3212	7.0385	7.0202	7.0205	109.5179	109.5156	109.5162
(1,2,+)	0.3264	0.3313	0.3313	7.0702	7.0706	7.0719	109.7618	109.7612	109.7638

The addition energy is conveniently used to show the shell closure that occurs at a specific electron number. The addition energy $\Delta\mu(N_e)$ is defined by

$$\Delta\mu(N_e)=\mu(N_e+1)-\mu(N_e), \tag{19}$$

where the chemical potential $\mu(N_e)$ is the increase of the ground state energy by adding one electron to the ground state of the N_e-1 system:

$$\mu(N_e)=E(N_e)-E(N_e-1). \tag{20}$$

Shell or half shell closure is reflected by a sudden increase of $\Delta\mu(N_e)$ at a certain N_e or the change of the differential capacitance given by $e^2/\Delta\mu(N_e)$. This is because the electron needs much energy when it fills an orbit across the degenerate orbits of a shell or goes beyond the half shell, due to Hund's rule. The addition energies of the harmonically confined electrons in 2D and 3D are compared in Figs. 5 and 6. In 2D the addition energy shows a large peak at $N_e=2$ and a smaller peak at $N_e=4$. The former corresponds to the filling of the $n=0,m=0$ orbit, while the latter is a reflection of the half shell filling of the degenerate orbits $n=0,m=\pm1$, which can be understood by Hund's rule. On decreasing ω the level spacing of the single-particle orbits becomes smaller and the correlation due to the Coulomb interaction takes over the shell structure. This explains why the peak at $N_e=2$ disappears for $\omega=0.1$. The behavior of the 3D addition energy is similar to the 2D case. One difference is that the half shell filling occurs at $N_e=5$ because the relevant orbit is $l=1$ and can accommodate six electrons.

The results for $N_e=5$ and $N_e=6$ are somewhat less accurate and the agreement between the SVM and the shell model is not as good as for $N_e<5$. The SVM seems to be more accurate than the shell model for weak confinement, where the role of the Coulomb interaction is more pronounced and it is more difficult to take the Coulomb correlation into account with the shell-model basis. At the same time it is easier to use the shell-model approach for larger systems (see Tables IX and X), while the SVM becomes very time consuming beyond $N_e=6$.

A general feature of the results is that the excited states change their level orders as the harmonic-oscillator strength changes, but the ground state always remains the same. We have very carefully tested this property and we do not find any level crossings with the ground state.

Other insights into the relation between the 2D and 3D systems can be gained by comparing the expectation values of the kinetic, confining, and Coulomb operators. Tables XI and XII show the contributions of the Coulomb, kinetic, and confinement parts of the Hamiltonian to the total energy. The contributions are nearly equal in the $\omega=0.5$ case. Just as one

TABLE VII. Energies of harmonically confined five-electron system in 3D. See the caption of Table V.

(L,S,π)	SVM	SM-eff $\omega=0.01$	SM	SVM	SM-eff $\omega=0.5$	SM	SVM	SM-eff $\omega=10$	SM
(0,3/2,−)	0.4804	0.5141	0.5165	8.9963	8.9979	9.0032	123.357	123.3539	123.3682
(2,1/2,−)	0.4858	0.5175	0.5203	9.0567	9.0526	9.0588	123.749	123.6960	123.7129
(1,1/2,−)	0.4880	0.5186	0.5211	9.0954	9.0919	9.0988	123.949	123.9287	123.9482
(1,3/2,+)	0.4869	0.5318	0.5359	9.3110	9.2969	9.3024	132.320	132.1385	132.1523
(0,1/2,+)	0.4931	0.5450	0.5525	9.4443	9.4355	9.4458	133.045	132.9021	132.9265
(1,3/2,+)	0.5108	0.5472	0.5537	9.7104	9.4701	9.3692	133.223	133.1205	133.1427
(2,1/2,+)	0.4950	0.5357	0.5406	9.3582	9.3528	9.3599	133.471	132.487	132.5026
(0,1/2,+)	0.5267	0.5561	0.5644	9.8766	9.5866	9.5990	134.204	133.8337	133.8658
(2,5/2,−)	0.4829	0.5232	0.5253	9.5919	9.5891	9.5914	140.973	140.9054	140.9105
(0,5/2,−)	0.4882	0.5306	0.5336	9.6626	9.6618	9.6648	141.270	141.2692	141.2762

TABLE VIII. Energies of harmonically confined six-electron system in 3D. See the caption of Table V.

(L,S,π)	SVM	SM-eff $\omega=0.01$	SM	SVM	SM-eff $\omega=0.5$	SM	SVM	SM-eff $\omega=10$	SM
(1,1,+)	0.703	0.797	0.815	12.038	12.064	12.079	157.701	157.415	157.451
(2,0,+)	0.743	0.801	0.819	12.080	12.101	12.118	157.910	157.643	157.681
(0,0,+)	0.714	0.805	0.822	12.128	12.159	12.178	158.080	157.991	158.034

expects in the strong confinement case ($\omega=10$) the kinetic and confinement energies are strongly enhanced, and the Coulomb energy is relatively small but not negligible. On the other hand, in the weak confining case the Coulomb interaction dominates.

The contribution of the confining interaction and thus the kinetic energy is of course larger in 3D. If the electrons did not interact then both the kinetic and the harmonic confinement energies would be increased 1.5 times in 3D compared to the 2D case. In the interacting case the kinetic and confinement energy increase is roughly 1.5 for $N_e=2$ and $N_e=3$. For more systems the increase is smaller. On the other hand, the Coulomb correlation energy is smaller in 3D than in 2D because there is more space available in 3D for the electrons.

C. Spherical square well

As an alternative to the harmonic confinement one can consider a spherical square well model of the 3D quantum dots. In this case the electrons are confined by a square well potential:

$$V_{\rm con}(r)=\begin{cases}-V_0, & r\leqslant R\\ 0, & r>R\ .\end{cases} \tag{21}$$

The square well potential is analytically solvable for the one-particle case. The eigenenergies E can be determined from the transcendental equation $\sqrt{V_0-|E|}\cot(\sqrt{2(V_0-|E|)}R)=-\sqrt{|E|}$ (for $l=0$, and atomic units used). Our SVM numerical approach almost exactly reproduces the analytically determined energies.

Spherical quantum-well-like quantum dots have been studied in Ref. 21. Unlike the harmonic-oscillator potential, the spherical well can hold only a certain number of electrons. The number of electrons that a spherical well can bind depends on V_0R^2. Figure 7 shows the energies of few-electron systems confined by a spherical square well potential in 3D as a function of the radius R. A spherical well can bind an electron only if $\pi^2/8<V_0R^2$. In our example $V_0=10$ and therefore the one-electron bound state appears when $0.35<R$. By increasing the radius the two-, three-, . . . , etc. electron systems may become bound in the well (see Fig. 7). This potential parameter was used in Ref. 21 to simulate quantum dots in GaAs/Al_{1-x}Ga$_x$As with $x\approx0.1$.

A comment is in order concerning the energy curves in Fig. 7 (and in Figs. 8 and 13 below). If the N_e-electron system has a bound ground state then our calculation converges to the energy of that state. If there is no bound state in a given potential then the energy converges to the lowest relevant threshold, which is in this case the energy of the (N_e-1)-electron system. In the figures the system is bound if the energy of the N_e-electron system is below that of the corresponding (N_e-1)-electron system. Strictly speaking, for unbound (N_e-electron) states the energies of the N_e-electron and (N_e-1)-electron systems should be equal. The convergence of the energy of the unbound N_e-electron system to the energy of the (N_e-1)-electron system is rather slow, so one needs many basis states to describe the ''free'' electron. Therefore the fact that the energy curves of the unbound states are above the corresponding thresholds is a consequence of our spatially limited basis. By using more basis states and by allowing them to go far outside the range of the confining interaction, one would get the same energy for the (N_e-1)- and the unbound N_e-electron systems.

We have found no ''phase transition'' in $N_e=2$ and $N_e=3$ electron systems. The authors of Ref. 21 investigated the energy of the lowest spin-polarized and spin-unpolarized $N_e=2$ and $N_e=3$ electron systems as a function of the radius of the square well. They found that beyond a certain radius the spin-polarized state becomes lower than the spin-

TABLE IX. Energies of harmonically confined seven-electron system in 3D. The SM is the shell-model calculation. Atomic units are used.

(L,S,π)	SM $\omega=0.01$	SM $\omega=0.5$	SM $\omega=10$
(1,1/2,−)	1.063	15.390	193.055
(1,3/2,−)	1.084	15.934	209.998
(3,5/2,−)	1.087	15.960	210.134
(0,1/2,+)	1.104	15.672	201.377
(2,3/2,+)	1.108	15.707	201.575
(3,3/2,+)	1.113	15.749	201.802

TABLE X. Energies of harmonically confined eight-electron system in 3D. See the caption of Table IX.

(L,S,π)	SM $\omega=0.01$	SM $\omega=0.5$	SM $\omega=10$
(0,0,+)	1.412	19.038	230.219
(0,2,+)	1.448	19.650	247.204
(2,1,+)	1.448	19.653	247.212
(1,1,−)	1.475	19.430	238.771
(3,1,−)	1.479	19.456	238.915
(2,0,−)	1.483	19.491	239.131
(2,1,−)	1.484	19.496	239.139

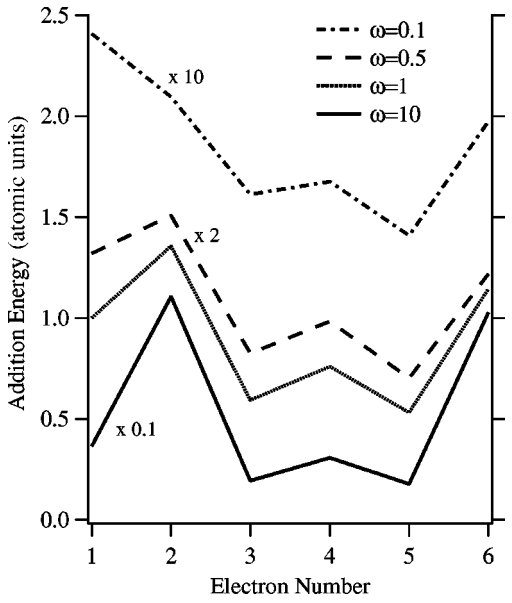

FIG. 5. Addition energy of harmonically confined electrons in 2D as a function of the electron number. ω is the frequency of the confining potential.

unpolarized ground state. We have very carefully investigated these systems and have not observed this ''paramagnetic to ferromagnetic phase transition.'' The same authors in a later paper[22] investigated a harmonically confined two-electron system and found that the spin-unpolarized to spin-polarized transition is most likely an artifact of the neglect of part of the electron-electron correlation in Hartree-Fock calculations.

We have increased the radius gradually (see Fig. 7). As the Coulomb repulsion decreases the energy of the system gets smaller and smaller, converging toward the energy of the noninteracting electrons in the quantum well. If there is no Coulomb interaction then the energy of the spin-polarized and -unpolarized electrons is the same, so on increasing the radius both converge to the same energy. In our present example ($V_0=10$) the energies of the lowest-lying spin-

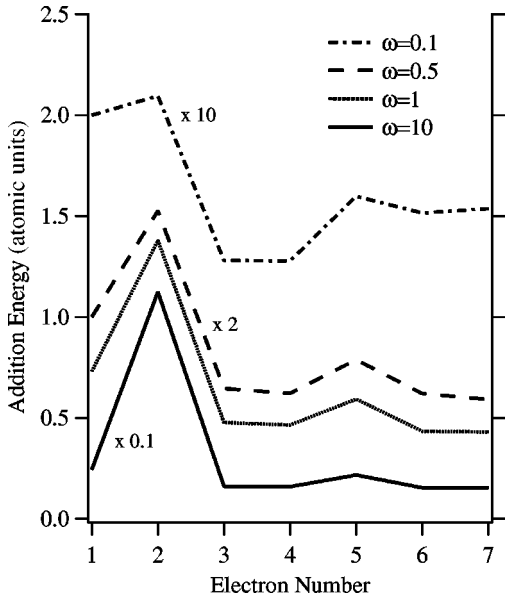

FIG. 6. Addition energy of harmonically confined electrons in 3D as a function of the electron number. ω is the frequency of the confining potential.

TABLE XI. Properties of harmonically confined 2D systems. Atomic units are used.

$N_e\,(M,S)$		$\omega=0.01$	$\omega=0.5$	$\omega=10$
2 (0,0)	$\langle H\rangle$	0.0738	1.659	23.652
	$\langle T\rangle$	0.0092	0.443	9.297
	$\langle V_{\mathrm{Coul}}\rangle$	0.0369	0.516	3.372
	$\langle V_{\mathrm{con}}\rangle$	0.0277	0.701	10.983
	η	0.9999998	0.9999995	0.9999998
3 (1,1/2)	$\langle H\rangle$	0.176	3.573	48.365
	$\langle T\rangle$	0.016	0.822	18.286
	$\langle V_{\mathrm{Coul}}\rangle$	0.096	1.286	7.858
	$\langle V_{\mathrm{con}}\rangle$	0.064	1.465	22.220
	η	0.9999972	0.9999984	0.9999981
4 (0,1)	$\langle H\rangle$	0.317	5.863	74.979
	$\langle T\rangle$	0.018	1.137	26.836
	$\langle V_{\mathrm{Coul}}\rangle$	0.186	2.391	14.163
	$\langle V_{\mathrm{con}}\rangle$	0.112	2.335	33.981
	η	0.999812	0.999921	0.999942
5(1,1/2)	$\langle H\rangle$	0.515	8.670	104.642
	$\langle T\rangle$	0.0196	1.421	34.931
	$\langle V_{\mathrm{Coul}}\rangle$	0.339	3.874	23.168
	$\langle V_{\mathrm{con}}\rangle$	0.159	3.376	46.543
	η	0.9992	0.9995	0.9991

TABLE XII. Properties of harmonically confined 3D systems. Atomic units are used.

$N_e\,(L,S,\pi)$		$\omega=0.01$	$\omega=0.5$	$\omega=10$
2(0,0,+)	$\langle H\rangle$	0.0792	2.0000	32.4486
	$\langle T\rangle$	0.0121	0.6644	14.4412
2 (0,0,+)	$\langle V_{\mathrm{Coul}}\rangle$	0.0366	0.4474	2.3776
	$\langle V_{\mathrm{con}}\rangle$	0.0304	0.8881	15.6299
	η	0.999999	0.999999	0.999999
3(1,1/2,−)	$\langle H\rangle$	0.1819	4.0132	61.1385
	$\langle T\rangle$	0.0192	1.1507	26.0867
	$\langle V_{\mathrm{Coul}}\rangle$	0.0957	1.1411	5.9763
	$\langle V_{\mathrm{con}}\rangle$	0.0671	1.7214	29.0755
	η	0.999991	0.999995	0.999999
4 (1,1,+)	$\langle H\rangle$	0.3161	6.3502	91.446
	$\langle T\rangle$	0.0229	1.5853	37.371
	$\langle V_{\mathrm{Coul}}\rangle$	0.1770	2.1174	11.132
	$\langle V_{\mathrm{con}}\rangle$	0.1163	2.6475	42.943
	η	0.999821	0.999891	0.999912
5(0,3/2,−)	$\langle H\rangle$	0.48041	8.9963	123.36
	$\langle T\rangle$	0.02501	1.9786	48.283
	$\langle V_{\mathrm{Coul}}\rangle$	0.27881	3.3562	17.808
	$\langle V_{\mathrm{con}}\rangle$	0.17660	3.6615	57.266
	η	0.99812	0.999671	0.999781

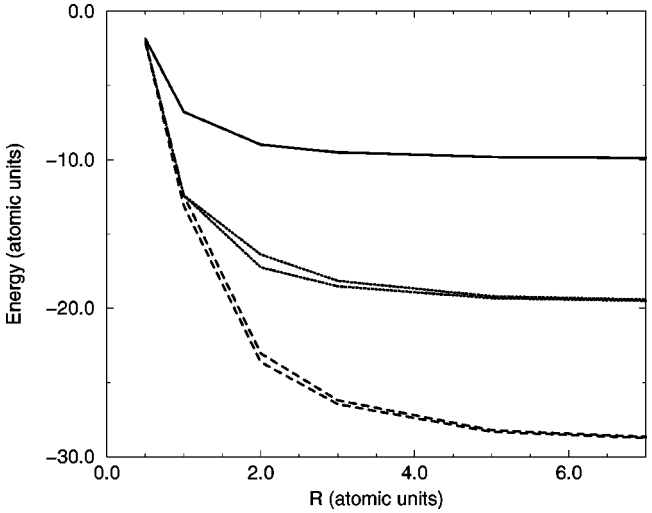

FIG. 7. Energies of $N_e=1$ (solid line), $N_e=2$ (dotted line), and $N_e=3$ (dashed line) electron systems in a spherical quantum well as a function of the radius of the well. Lower dotted line, the ground state $(0,0,+)$; upper dotted line, the excited state $(1,1,-)$; lower dashed line, the ground state $(1,1/2,-)$; upper dashed line, the first excited state $(1,3/2,+)$.

polarized and -unpolarized states are nearly degenerate beyond $R=15$, but we observe no level crossing between them.

D. Cylindrical well: ''Quantum cylinder''

In this section we present a calculation for a cylindrical quantum dot. A similar case was considered in Ref. 23 in an unrestricted Hartree-Fock framework. The confinement is defined as

$$V_{\rm con}(\mathbf{r})=\begin{cases} -V_0 & \text{if } (x^2+y^2)^{1/2}<R \text{ and } |z|<a \\ 0 & \text{otherwise.} \end{cases} \tag{22}$$

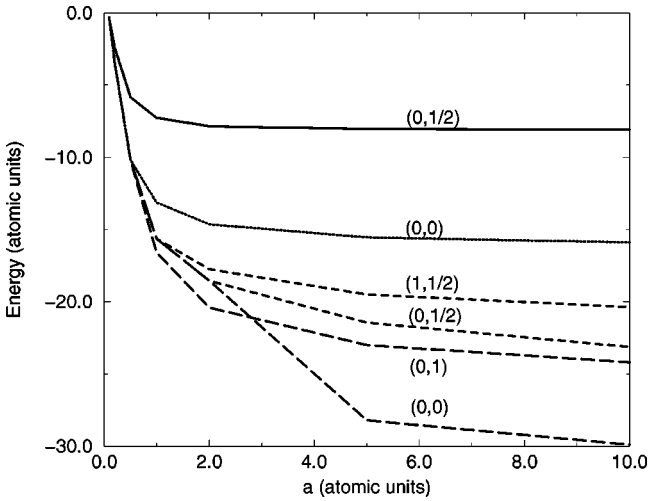

FIG. 8. Energy of $N_e=1$ (solid line), $N_e=2$ (dotted line), $N_e=3$ (dashed line), and $N_e=4$ (long dashed line) electron systems in a cylindrical quantum well as a function of the height of the cylinder. ($V_0=10$ and atomic units are used.)

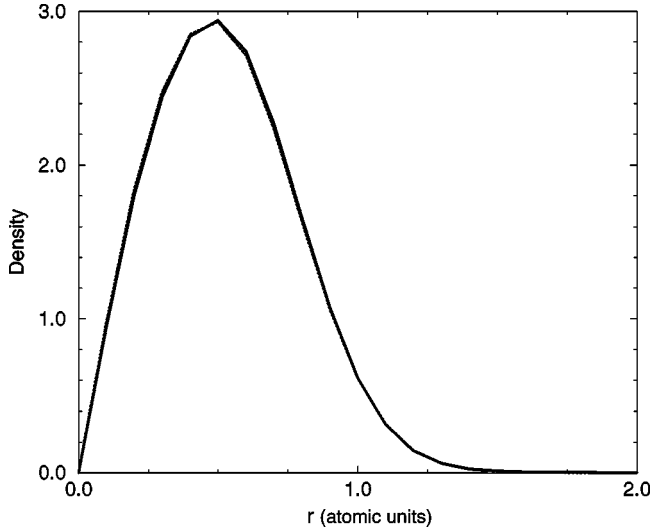

FIG. 9. Singlet (solid line) and triplet (dotted line) radial density distributions of two electrons in a cylindrical quantum dot ($a=10$). The probability density distribution (dimensionless) is defined in Eq. (23) and normalized to the number of electrons.

In this case the spherical symmetry is broken, and only the z component of the orbital angular momentum is conserved. We have to use the DCG basis functions that were introduced for magnetic field. The state of this system is specified by the total magnetic quantum number M, total spin S, and π_z, the parity along the ''z'' direction. Our basis is restricted to even parity states and this last quantum number is dropped in the following.

First we consider a model potential with $V_0=10$ and $R=1$ and change the ''thickness'' of the dot (the height of the cylinder) from $a=10$ to $a=0$ (in a.u.). In this way we transform the system from a rodlike ($a=10$) geometry to a 2D disk ($a=0$). Just as in the case of the spherical quantum well a quantum cylinder can bind only a certain number of electrons, depending on the potential parameters V_0, R, and a. The energy dependence on the thickness of the cylindrical dot for $N_e=1-4$ electron systems is presented in Fig. 8. The figure shows that, as one expects, the cylinder can hold more and more electrons as the size (in our case the height) increases. The really interesting thing here is that the order of the energy levels also depends on the height of the cylinder. For long, rodlike cylinders the ground state tends to be the $M=0$ orbital angular momentum state. This probably means that the electrons are equidistantly positioned along the z axis. On decreasing the height we approach a disklike geometry which is somewhat similar to the 2D harmonic confinement discussed earlier. And, indeed, the level order changes (see Fig. 8) and one has the same level order as in the 2D harmonic confinement case. In this way we have found an interesting transition: On decreasing the height of the cylinder the $(0,1/2)$ and $(1,1/2)$ $N_e=3$ electron [also the $(0,0)$ and $(0,1)$ $N_e=4$ electron] ground/excited states change their order.

Figures 9 and 10 show the density of the $N_e=2$ electron system in a ''long'' cylinder ($a=10$) along the radius and along the symmetry axis, respectively. The density is defined as

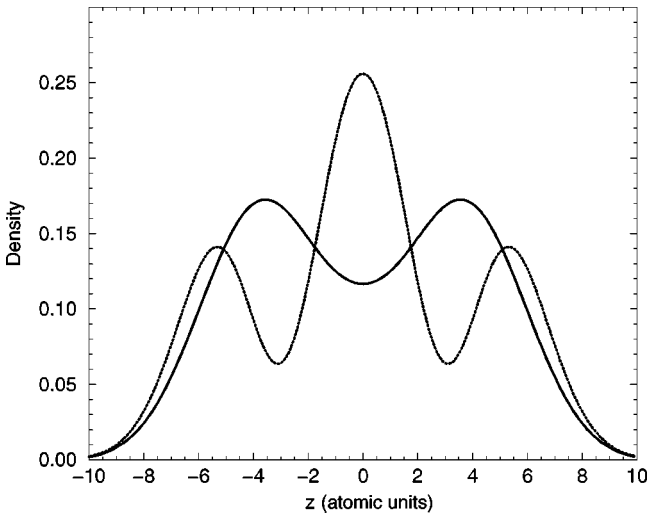

FIG. 10. Singlet (solid line) and triplet (dotted line) density distributions along the z direction of two electrons in a cylindrical quantum dot ($a=10$). See the caption of Fig. 9 also.

$$\rho(\mathbf{r})=\langle\Psi|\sum_{i=1}^{N_e}\delta(\mathbf{r}_i-\mathbf{R}-\mathbf{r})|\Psi\rangle, \tag{23}$$

and the radial density is obtained by integrating this quantity along the z direction. The density is normalized to the number of electrons. The radial density distributions of the triplet (1,1) and singlet (0,0) states are very similar. Both peak around 0.5 a.u. and the tail goes a little bit outside the cylinder. The density of the triplet and the singlet states in the z direction (obtained by integrating the density over the x and y variables), however, are very different as shown in Fig. 10. The cylinder is so long that the two electrons can be far away from each other to minimize the Coulomb repulsion and the density tail hardly goes outside the cylinder.

E. ''Quantum ring''

Ringlike nanostructures have been grown by electron-beam lithography.[34] The electronic and magnetic properties of a single-electron quantum ring were studied in Ref. 35. We restrict our attention to a pure 2D case. An additional confining interaction in the z direction would cause no extra difficulty in our approach. The confinement in this case is defined as

$$V_{\mathrm{con}}(\rho)=\begin{cases}0, & \rho<r_1\\ -V_0, & r_1\leqslant\rho\leqslant r_2\\ 0, & \rho>r_2.\end{cases} \tag{24}$$

This describes a square well potential in a ring between r_1 and r_2 on the xy plane.

The number of electrons bound in a ringlike potential, as in the previous cases, depends on the parameters (V_0,r_1,r_2) of the potential. An example of the energy levels in the model potential is presented in Fig. 11. The maximum number of electrons this potential can bind is $N_e=4$. In the four-electron case the lowest state is the $(M,S)=(0,1)$ state just as in the case of 2D harmonic confinement. In the present model potential the first excited state (0,0) is not bound with respect to the three-electron threshold.

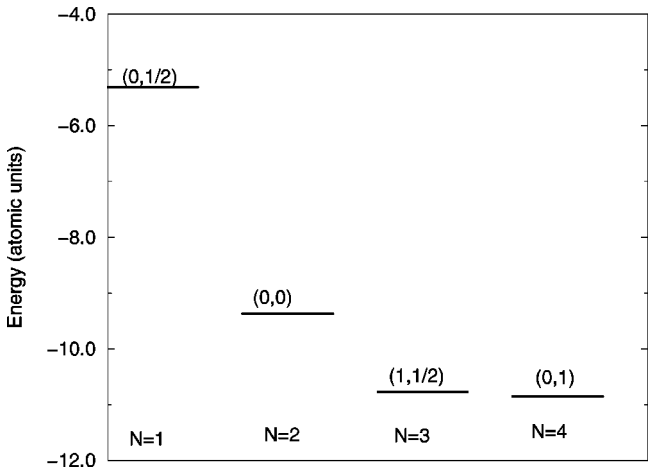

FIG. 11. Energy levels of $N_e=1-4$ electron quantum rings. The parameters of the potential are $V_0=10$, $r_1=0.5$, and $r_2=1$. Atomic units are used.

This density distribution can easily be manipulated by a perpendicular magnetic field. The magnetic field acts as a confining harmonic-oscillator potential on the xy plane. On increasing the strength of the magnetic field, the density distribution starts to move inward as shown in Fig. 12. In a certain very narrow region of the magnetic field strength it has two peaks: an outer peak centered in the ring and an inner peak that is inside the harmonic confinement induced by the magnetic field. If the magnetic field is stronger than a given value then the electron moves inside the harmonic confinement. This geometry gives us the possibility of moving the electron from one well-defined position to another by switching on and off the magnetic field. Notice that we have

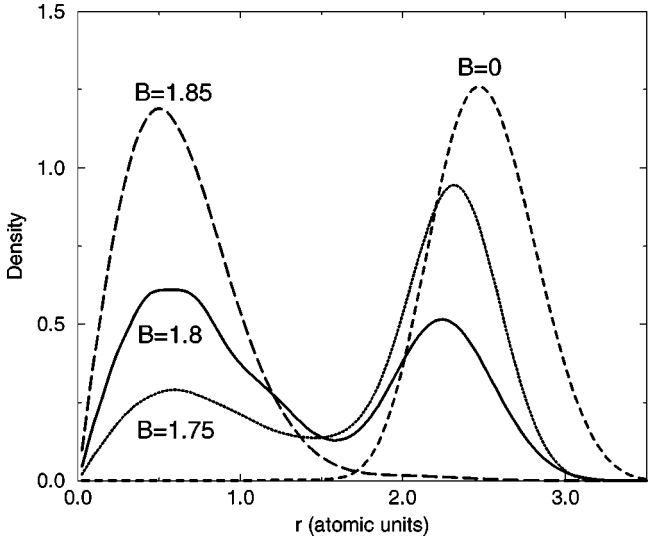

FIG. 12. Density distribution in a single-electron quantum ring as a function of the magnetic field. The strength of the magnetic field is indicated next to the corresponding density distribution. The parameters of the potential are $V_0=10$, $r_1=2$, and $r_2=3$. Atomic units are used. See the caption of Fig. 9 also.

two sharply separated peak positions in this case. In the case of the previously studied harmonic or spherical square well confinement the density distribution also moves toward the origin in the magnetic field. In that case, however, what we see is more like a ''shrinking'' of the density distribution on the xy plane. The change is more drastic in the case of the quantum ring. The peak of the distribution shifts from one position to another.

IV. DISCUSSION

The properties of artificial atoms created by confining electrons in quantum dots of different geometries are qualitatively very similar. The electrons occupy the single-particle orbits defined by the confining interaction. The occupancy is determined by the Pauli principle and the minimization of the Coulomb energy. In different confining potentials the energy levels are different but the essential features are very similar.

The confining interactions considered in this paper depend on one or more parameters (harmonic-oscillator width, radius and strength of square well, etc.). We have studied the dependence of the energy levels on these parameters. One intriguing property those we have found is that in spherically symmetric systems the ground state remains the same for any values of the parameters. Its energy level does not cross with those of the excited states. At the same time, the order of energy levels of the excited states frequently changes depending on the parameters of the confining interactions. A change of symmetry of the ground state of a spherical quantum well has been reported in Ref. 21. We have investigated few-electron systems in spherical quantum wells of different parameters but we have not observed any similar change. This confirms that such a change of energy levels might be an artifact of Hartree-Fock calculations.[22] Our calculation predicts that the ground state is in accordance with Hund's rule for any parameter values and there is no transition from spin-unpolarized to spin-polarized states.

A change of the ground state would give us an interesting possibility. In a two-electron system, for example, the ground state is a spin singlet, and the first excited state is a spin triplet. This two-state system may serve as a ''qubit,'' an elementary gate for a quantum dot quantum computer. One would prepare a dot with singlet ground and triplet excited states and a second one, with different geometry, where it is the other way around. The electrons can be moved from one dot to the other by an external electric field, for example, switching from $S=0$ to $S=1$. The calculations show, however, that no matter how we change the geometry, the ground state does not change for spherically symmetric systems.

If the spherical symmetry is broken, for example by a magnetic field or by a cylindrically symmetric confining potential, then the ground state and excited state energy levels may cross each other. The fact that the magnetic field changes the order of energy levels has been studied frequently. In this paper we have presented a method that very accurately predicts the level crossing as a function of the strength of the magnetic field.

The cylindrical quantum dot is a very interesting example where the order of energy levels depends on the height of the quantum dot. In a disklike cylinder the ground state obeys Hund's rule, but for a longer cylinder, typically when the height of the cylinder is larger than its diameter, Hund's rule is violated. It would be interesting to look for experimental evidence showing that the ground state of a cylindrical three-(four-) electron quantum dot is an $(M,S)=(1,1/2)$ $[(M,S)=(0,1)]$ state if the height of the cylinder is small and becomes an $(M,S)=(0,1/2)$ $[(M,S)=(0,0)]$ state on increasing the height of the cylinder.

Harmonically confined electron systems in 2D have attracted enormous attention. In this work we have also calculated 3D electron systems in harmonic confinement. Comparison of the 2D and 3D cases shows the effects of the quantum well confinement in the z direction in quantum dots. For the same harmonic-oscillator strength the electrons are somewhat farther from each other in 3D than in 2D, resulting in a smaller Coulomb energy in 3D. The energy difference between the 2D and 3D geometries is predominantly due to the confinement and the kinetic energy. The qualitative features of the 2D and 3D systems are very similar in the case of the few-electron systems investigated here. One can make an easy correspondence between the orbital and spin quantum numbers of the energy levels in 2D and 3D. The applicability of our method was tested by calculations for very different confining strengths. The accuracy is slightly worse for the weak confining region where one needs more basis functions to achieve convergence, but it is fairly good as one can judge by the virial factor and by comparing with the results of different methods. In the weak confining region ($\omega=0.01$; see Tables XI and XII) the contribution of the kinetic energy is fairly small compared to that of the Coulomb and confining interactions. This suggests the existence of a Wigner-crystal-like structure in both 2D and 3D. Contrary to the prediction of Refs. 15 and 17 we find that the ground state of the $N_e=4$ system obeys Hund's rule.

We have also investigated an example of a ringlike quantum dot in a magnetic field. This geometry offers an interesting possibility. In the case of zero magnetic field the electrons are distributed along the ring. By applying the magnetic field perpendicularly to the plane of the ring the electrons can be completely moved from the ring to the vicinity of the origin. Thus one may have the electrons in two very well-separated regions.

The major difference between the harmonic and square well confinements (cylindrical, spherical, and ring) is that the harmonic potential can bind any number of electrons. The number of electrons bound in the square well case is finite and strongly depends on the parameters of the potential. In that case one can predict how many electrons can be bound in a certain quantum dot, that is, the ''capacity''[36] of the dot. This is expected to be a more realistic model of quantum dots.

The concrete potential parameters and the potential itself can only be determined experimentally. In this work we have tried to follow ''experimentally inspired'' and widely used potentials and parameters. The aim of this work was to demonstrate the wide range of applicability of the method and the investigation of different properties of various artificial

atoms. The general features of experimental findings may be reasonably well described by the potential models considered here. In the present approach one assumes a Hamiltonian that models the quantum dot and we try to solve this well-defined quantum mechanical problem in a careful manner. There are of course many things that may limit the applicability of our model Hamiltonian, but some of the phenomena that are experimentally observed can be understood by such model calculations, and we hope that some of the predictions of such models can be experimentally observed.

The accuracy presented here is very useful and important in the weakly confined (but strongly correlated) regime where otherwise it is difficult to predict the ground state, etc. One should also mention that the comparison of various methods for these quantum mechanical problems greatly helps in testing and development of different quantum mechanical many-body approaches. A nice example can be found in Ref. 33, where the solution of few-electron quantum dot problems helps to test the Faddeev method, which was developed for nuclear few-body systems.

In summary, we have presented a large scale variational approach to describe the spectra and other properties of artificial atoms. Different (parabolic, cylindrical, spherical, and ring-like) confining interactions have been investigated. The effects of magnetic field have also been studied. One of the aims of this paper was to introduce the method and test its capabilities on various models of quantum dots used in the literature. Future work to investigate double quantum dots is under way.

ACKNOWLEDGMENTS

The work of K.V. was sponsored by the U.S. Department of Energy under Contract No. DE-AC05-00OR22725 with the Oak Ridge National Laboratory, managed by UT-Battelle, LLC, and OTKA Grant No. T029003 (Hungary). Y.S. was supported in part by the Matsuo Foundation and the JSPS-HAS cooperative research program. J.U. was supported by JSPS. The work of P.N. was performed under the auspices of the U.S. Department of Energy at the University of California Lawrence Livermore National Laboratory under Contract No. W-7405-Eng-48. P.N. also acknowledges support in part by the NSF Grant No. PHY96-05192.

*Corresponding author. Email address: vargak@ornl.gov

†On leave from Nuclear Physics Institute, Academy of Sciences of the Czech Republic, 250 68 Rez near Prague, Czech Republic.

[1] R. C. Ashoori, H. L. Stormer, J. S. Winer, L. N. Pfeiffer, K. W. Baldwin, and K. W. West, Phys. Rev. Lett. **71**, 613 (1993).

[2] S. Tarucha, D. G. Austing, T. Honda, R. J. van der Hage, and L. P. Kouwenhoven, Phys. Rev. Lett. **77**, 3613 (1996).

[3] M. Grundmann, O. Stier, and D. Bimberg, Phys. Rev. B **52**, 11 969 (1995).

[4] L. Jacak, P. Hawrylak, and A. Wojs, *Quantum Dots* (Springer-Verlag, Berlin, 1998).

[5] N. A. Bruce and P. A. Maksym, Phys. Rev. B **61**, 4718 (2000).

[6] P. Hawrylak and D. Pfannkuche, Phys. Rev. Lett. **70**, 485 (1993).

[7] P. Hawrylak, Phys. Rev. Lett. **71**, 3347 (1993).

[8] A. Wojs and P. Hawrylak, Phys. Rev. B **53**, 10 841 (1996); **55**, 13 066 (1997).

[9] P. A. Maksym and T. Chakraborty, Phys. Rev. Lett. **65**, 108 (1990); J. J. Palacios, L. Moreno, G. Chiappe, E. Louis, and C. Tejedor, Phys. Rev. B **50**, 5760 (1994).

[10] M. Fujito, A. Natori, and H. Yasunaga, Phys. Rev. B **53**, 9952 (1996).

[11] H. M. Muller and S. Koonin, Phys. Rev. B **54**, 14 532 (1996).

[12] C. Yannouleas and U. Landman, Phys. Rev. Lett. **82**, 5325 (1999); **85**, 1726 (2000); **85**, 2220 (2000).

[13] M. Koskinen, M. Manninen, and S. M. Reimann, Phys. Rev. Lett. **79**, 1389 (1997).

[14] K. Hirose and N. S. Wingreen, Phys. Rev. B **59**, 4604 (1999).

[15] F. Bolton, Phys. Rev. B **54**, 4780 (1996).

[16] A. Harju, V. A. Sverdlov, R. M. Nieminen, and V. Halonen, Phys. Rev. B **59**, 5622 (1999).

[17] F. Pederiva, C. J. Umrigar, and E. Lipparini, Phys. Rev. B (to be published).

[18] J. Shumway, L. R. C. Fonseca, J. P. Leburton, R. M. Martin, and D. M. Ceperley (unpublished).

[19] D. J. Dean, M. R. Strayer, and J. C. Wells, cond-mat/9912310 (unpublished).

[20] R. Egger, W. Häusler, C. H. Mak, and H. Grabert, Phys. Rev. Lett. **82**, 3320 (1999).

[21] B. Szafran, J. Adamowski, and S. Bednarek, Physica E (Amsterdam) **4**, 1 (1999).

[22] B. Szafran, J. Adamowski, and S. Bednarek, Physica E (Amsterdam) **5**, 185 (2000).

[23] B. Szafran, J. Adamowski, and S. Bednarek, Phys. Rev. B **61**, 1971 (2000).

[24] R. Egger, W. Häusler, C. H. Mak, and H. Grabert, Phys. Rev. Lett. **82**, 3320 (1999).

[25] J. Harting, O. Mülken, and P. Borrmann, cond-mat/0002269 (unpublished).

[26] Y. Suzuki and K. Varga, *Stochastic Variational Approach to Quantum Mechanical Few-Body Problems* (Springer-Verlag, Berlin, 1998).

[27] K. Varga and Y. Suzuki, Phys. Rev. C **52**, 2995 (1995).

[28] P. Navrátil and B. R. Barrett, Phys. Rev. C **57**, 562 (1998); **59**, 1906 (1999).

[29] P. Navrátil, G. P. Kamuntavičius, and B. R. Barrett, Phys. Rev. C **61**, 044001 (2000).

[30] J. P. Vary and D. C. Zheng, Many-fermion-dynamics shell-model computer code, Iowa State University, 1994.

[31] K. Varga (unpublished).

[32] M. Taut, Phys. Rev. A **48**, 3561 (1993).

[33] P. Navrátil, B. R. Barrett, and W. Glöckle, Phys. Rev. C **59**, 611 (1999).

[34] G. E. Philipp *et al.*, in *Diagnostic Techniques for Semiconductor Materials Processing II*, edited by S. W. Pang O. J. Glembocki, F. H. Pollak, F. Celli, and C. M. S. Torres MRS Symposia Proceedings No. 406 (Materials Research Society, Pittsburgh, 1996), p. 307.

[35] Z. Barticevic, M. Pacheco, and A. Latge, Phys. Rev. B **62**, 6963 (2000).

[36] S. Bednarek, B. Szafran, and J. Adamowski, Phys. Rev. B **59**, 13 036 (1999).